

# Design, fabrication and initial test of a novel 3D-Trench sensor utilizing 8-inch CMOS compatible technology

Manwen Liu, Huimin Ji, Wenzheng Cheng, Le Zhang, Zheng Li, Bo Tang, Peng Zhang, Wenjuan Xiong, Trevor Vickey, E. Giulio Villani, Zhihua Li, Dengfeng Zhang, and Jun Luo

**Abstract**—The 3D silicon sensor has demonstrated excellent performances (signal collection, detection efficiency, power consumption, etc.) comparable or even better with respect to the traditional planar sensor of the ATLAS Detector at the Large Hadron Collider (LHC), especially after the high irradiation fluence, mainly due to the shorter drift length of the generated carriers. These characteristics have made it the most attractive technology for the detection and track reconstruction of charged particles for the High Energy Physics (HEP). In addition, its application is also being explored in astronomy, microdosimetry and medical imaging. This paper will present the design and fabrication of a novel 3D-Trench sensor which features an enclosed deep trench surrounding the central columnar cathode. This novel sensor has been fabricated on the 8 inch COMS pilot line at the Institute of Microelectronics of the Chinese Academy of Sciences (IMECAS) where ultra-narrow etch width of  $0.5 \mu\text{m}$  and the ultra-high depth-to-width ratio (aspect ratio) ( $>70$ ) have been achieved. Its preliminary simulation and characterization results including electrostatic potential, electric field, Current-Voltage (IV), Capacitance-Voltage (CV), Charge Collection Efficiency (CCE) and Timing Performance before irradiation will be presented in this paper.

**Index Terms**—Silicon 3D-Trench Sensor, 8 inch Wafer, Pixel

## I. INTRODUCTION

SINCE its proposal by S. Parker et al. in 1998 [1], [2], the 3D sensor has undergone extensive research and has found diverse applications in high-energy physics experiments (the High-Luminosity LHC) [3]–[5], microdosimetry for proton and heavy-ion treatment [6]–[8], X-ray spectroscopy in computed tomography (CT) scanners [9], and astroparticle detection in deep space radiation environments [10]. These applications benefit from the sensor's outstanding features, including short collection distances, fast collection times, low depletion voltages, radiation hardness, and the ability to provide position resolution of the order of microns. Furthermore,  $\text{SiO}_2$  3D trench-isolation technology has been employed in avalanche diodes to achieve small pixel pitch and high fill-

This paper is submitted on December 18, 2024. This work is supported by the National Key R&D Program of China under Grant 2023YFF0719600, General Program of National Natural Science Foundation of China under Grant 12375188, and the Science and Technology Facilities Council (STFC) of United Kingdom under grants ST/S000747/1 and ST/W000547/1. We are also grateful for the support with equipment and technical personnel by the IMECAS, the School of Mathematical and Physical Sciences of the University of Sheffield, and the Rutherford Appleton Laboratory. (Corresponding author: Manwen Liu, Zhihua Li and Dengfeng Zhang.)

Manwen Liu and Zhihua Li are with the Key Laboratory of Fabrication Technologies for Integrated Circuits of Chinese Academy of Sciences and the Institute of Microelectronics of Chinese Academy of Sciences, Beijing 100029, China (e-mail: liumanwen@ime.ac.cn, lizhihua@ime.ac.cn).

Dengfeng Zhang is with the School of Mathematical and Physical Sciences, The University of Sheffield, Sheffield, S10 2TN, UK (e-mail: dengfeng.zhang@cern.ch).

factor, enhancing their performance in imaging and particle detection [11], [12].

In the past two decades, institutes such as IMB-CNM [13]–[15], SINTEF [3], [16]–[18], University of Trento [17], [19], INFN [20], FBK [21]–[24], BNL [25], and others have conducted extensive research on 3D sensors with varying electrode thicknesses, geometries, aimed at wide ranges of scientific applications. The aforementioned research has provided valuable design insights and techniques for the fabrication process for the development of 3D sensors aimed at different applications. Recent investigation has shown excellent timing resolution of less than 100 ps [26].

The fabrication process of 3D sensors presents several challenges, such as the precise shape of the electrodes, their size and depth-to-width ratio (aspect ratio) of the electrodes. For example, the ATLAS Phase-II upgrade for the HL-LHC [5] introduces additional complexities, with the new ITk (Inner Tracker) module necessitating a reduction in pixel unit size and substrate thickness [27], [28]. Furthermore, the production of wafers with thicknesses below 100 micrometers presents significant fabrication challenges, including wafer bending and alignment, posing new difficulties to the manufacturing process.

In this work, an innovative 3D-Trench sensor was designed and fabricated on the epitaxial layer (EPI) grown on 8-inch wafer. This design maintains a thin effective volume while mitigating the fabrication risks associated with thin silicon substrates. The sensor was fabricated using the 8-inch CMOS process platform at the Institute of Microelectronics of the

Chinese Academy of Sciences (IMECAS). Notably, we have achieved an aspect ratio of 70:1 with an electrode width of  $0.5 \mu\text{m}$ , significantly enhancing the sensor's fill factor. The manufacture technology based on the 8-inch CMOS compatible process lays a solid foundation for future large-scale production and application due to its scalability, flexibility, cost-effectiveness, maturity, and compatibility. Additionally, the electrical isolation of the 3D trench electrode simplifies the guard ring design compared to traditional 2D or 3D sensors. The designed 3D-Trench sensor exhibits low depletion voltage and fast signal collection. Our theoretical analysis is grounded in the frameworks of the 3D-Trench electrode sensor [25] and near-hemispherical electrode sensor [29], providing a robust foundation for our findings.

This paper is organized as follows. Section II gives a description of the design of the silicon 3D-Trench sensor. In section III, a description of the fabrication process of the devices will be given. Section IV will present test and simulation results, including Current-Voltage (IV), Capacitance-Voltage (CV), Charge Collection Efficiency (CCE), Time Resolution and Rise Time. Finally, in section V, preliminary conclusions and a description of the next steps for this project will be given.

## II. DESIGN OF THE 3D-TRENCH SENSOR

In the novel design of the 3D-Trench sensor, the columnar cathode is surrounded by a deeply etched trench, instead of columnar anodes, as in traditional 3D pixel sensor [1]. The shape of the trench can be square or circular. Fig. 1 shows the schematic of the 3D-Trench sensor. The 3D-Trench sensor devices are fabricated on 8-inch silicon wafer, the sensitive layer is a high resistivity  $p$ -type epitaxial layer with a thickness of  $30 \mu\text{m}$ , grown on low-resistivity  $p$ -type substrate. Both the enclosed 3D-Trench anode and the central columnar cathode are achieved by etching the epitaxial layer from the front side. The 3D-Trench anode will fully penetrate the epitaxial layer and into the substrate by  $\sim 5 \mu\text{m}$ , but the etching for the central columnar cathode will stop at 5 to  $10 \mu\text{m}$  from the substrate. More details on the fabrication are presented in Section III. Both columnar and trench electrodes have a width of  $0.5\text{--}2 \mu\text{m}$  with an achieved aspect ratio of 70:1 or larger, which suppresses the dead areas significantly. In this design, the  $pn$  junction is formed near the central electrode and the depletion region develops from the central cathode up to the trench wall.

We have designed different device layouts differing in the shape of the 3D trench and pixel size. Fig. 2 shows two example layouts: A21-21 ( $5 \times 5$  pixel array with the pixel size of  $35 \times 35 \mu\text{m}$ ) and A21-43 ( $3 \times 3$  pixel array with the pixel size of  $25 \times 25 \mu\text{m}$ ). Their details are listed in Table I.

**TABLE I:** Layouts of 3D-Trench pixel devices: A21-21 and A21-43.

Layout	Trench Shape	Electrode Width [ $\mu\text{m}$ ]	Array	Pixel Size [ $\mu\text{m}$ ]
A21-21	Square	0.5	$5 \times 5$	$35 \times 35$
A21-43	Square	0.5	$3 \times 3$	$25 \times 25$

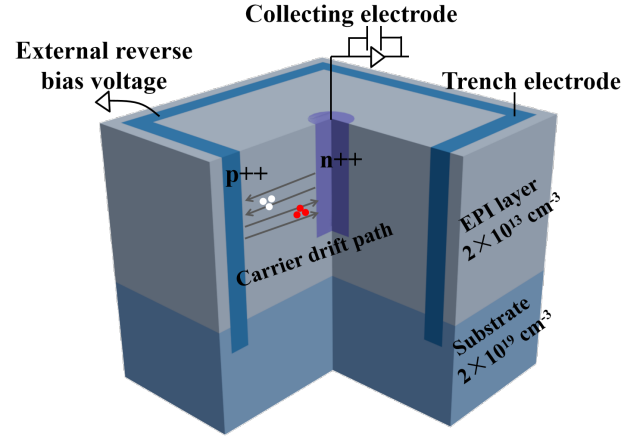


**Fig. 1:** The schematic of the 3D-Trench Sensor.

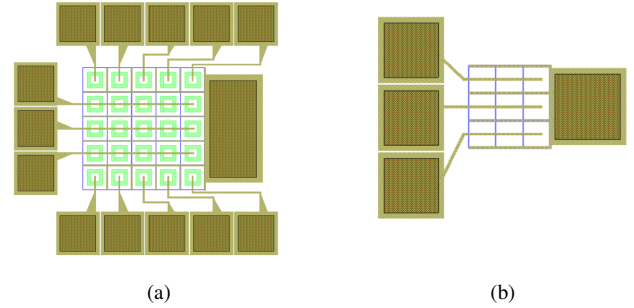


**Fig. 2:** Layouts of the 3D-Trench pixel array, (a) A21-21:  $5 \times 5$  pixel array with the pixel size of  $35 \times 35 \mu\text{m}$ , (b) A21-43:  $3 \times 3$  pixel array with the pixel size of  $25 \times 25 \mu\text{m}$ .

## III. FABRICATION OF THE 3D-TRENCH SENSOR

The 3D-Trench sensors were fabricated on 8" EPI wafer based on the  $0.5 \mu\text{m}$  CMOS technology at IMECAS in Beijing. The epitaxial layer is  $p$ -type silicon with a doping concentration of  $2 \times 10^{13} \text{ cm}^{-3}$  and has a thickness of  $30 \mu\text{m}$ . The substrate is  $p$ -type silicon with a thickness of  $695 \mu\text{m}$  and a doping concentration of  $2 \times 10^{19} \text{ cm}^{-3}$ .

The full fabrication process flow is shown in Fig. 3. The fabrication started with the thermal growth of  $700 \text{ nm}$  oxide layer on the wafer. This oxide layer provides surface passivation and serves as a hard mask for the subsequent silicon deep etch process. Next, a layer of photoresist was spin-coated onto the wafer surface, followed by the photolithography and etching procedures to open a  $0.5\text{--}2 \mu\text{m}$  width window through the oxide for the trench etching of the next step. Next, the Bosch Deep Reactive Ion Etching (DRIE) procedure was performed in the windows opened in the previous step to achieve a  $35 \mu\text{m}$  deep trench. After the trench etching, the in-situ boron diffusion was performed in the etched trench to form a  $p$ -type enclosed 3D anode and filled the trench with conductive polysilicon. Thereafter, the polysilicon on the surface was removed and the 3D-Trench anode was obtained. Before etching the central pillar for the cathode, another oxide layer was deposited on the surface using the Plasma-Enhanced Chemical Vapor Deposition (PECVD) technique. The same procedures

were then performed to form the central columnar cathode, except that the etching depth of the central pillar was shallower ( $25\ \mu\text{m}$ ) and the phosphorus diffusion was performed to form a *pn* junction. The last steps consisted of stripping the photoresist on the surface and repeat the photolithography for the electrode metal contact formation. were to strip the photoresist on the surface and repeat the photolithography for electrode metal contact. The electrode contact was formed by the tungsten (W) deposit and magnetron sputtering of Al.

The final fabricated wafer is shown in Fig. 4a. Fig. 4b shows the Scanning Electron Microscopy (SEM) micrography of the etched trench, showing the achieved minimum trench width of  $\sim 0.5\ \mu\text{m}$  and a maximum aspect ratio exceeding 70. Fig. 4c and 4d show the microphotographs of the  $5\times 5$  pixel array with pixel size of  $35\times 35\ \mu\text{m}$  and  $3\times 3$  pixel array with pixel size of  $25\times 25\ \mu\text{m}$ , respectively.

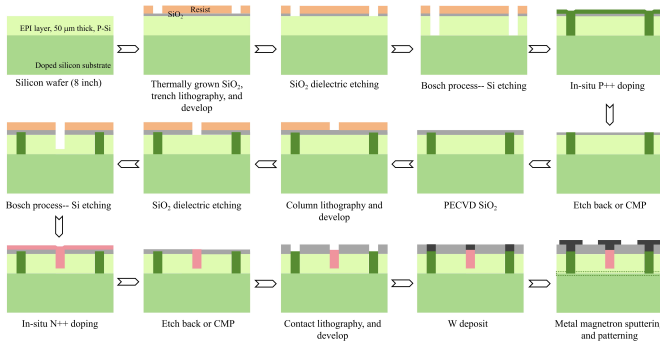


Fig. 3: The fabrication process flow of the 3D-Trench Sensor at IMECAS.

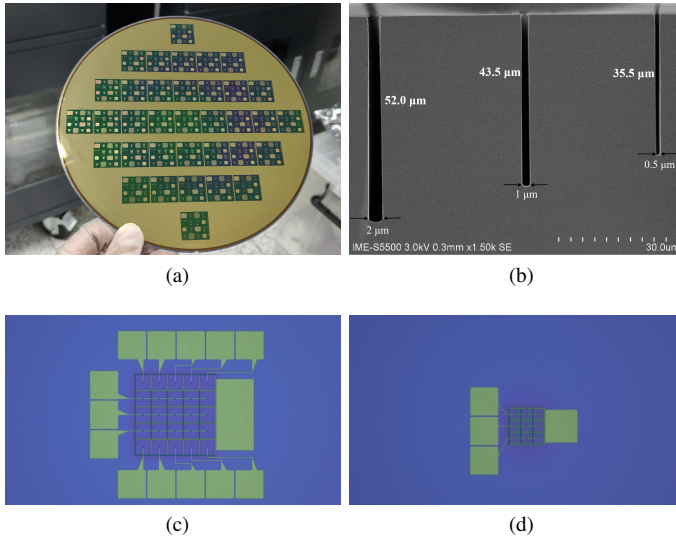


Fig. 4: (a) The final fabricated 8'' wafer at IMECAS, (b) the SEM micrograph in cut view of the 3D trench, (c) the microphotographs of the surface of A21-21:  $5\times 5$  pixel array with pixel size of  $35\times 35\ \mu\text{m}$  and (d) A21-43:  $3\times 3$  pixel array with pixel size of  $25\times 25\ \mu\text{m}$ .

#### IV. CHARACTERIZATION MEASUREMENT AND SIMULATION OF THE DEVICE

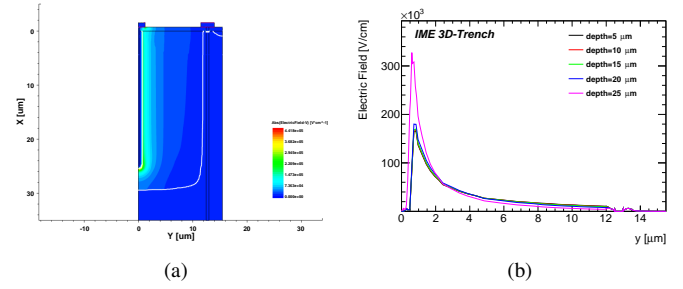


Fig. 5: (a) The simulated distributions of the electric field and (b) its profile in radial direction at various depths of the 3D-Trench Sensor at the reverse bias voltage of 40 V.

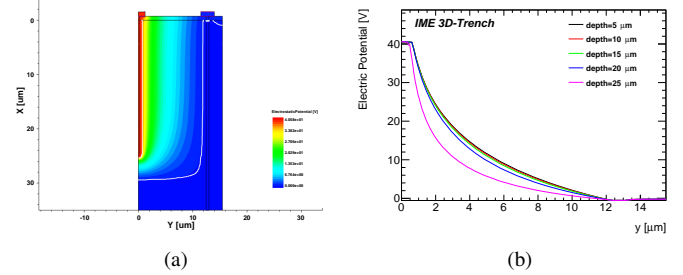


Fig. 6: (a) The simulated distributions of the electric potential and (b) its profile in radial direction at various depths of the 3D-Trench Sensor at the reverse bias voltage of 40 V.

##### A. Electrical characteristics of the 3D-Trench sensor

Simulations have been performed using the Synopsys TCAD [30]. In our simulation, a 3D simulated structure in TCAD was obtained from a 2D one by performing a rotation along the *x* vertical axis. Fig. 5 and 6 show the simulated distribution of the electric field and potential of a 3D-Trench Sensor with the pixel diameter of  $25\ \mu\text{m}$  at the reverse bias voltage of 40 V, a voltage sufficient to guarantee full depletion. From the pictures it is seen that the maximum strength of the electric field is located near the central cathode, with the largest value of the field near the bottom, due to the sharpness of the junction's edge. The largest value is  $\sim 4.4\times 10^5\ \text{V/cm}$ , high enough to ignite impact ionisation.

The Current-Voltage (IV) and Capacitance-Voltage (CV) characteristics in the reverse biasing mode of the 3D-Trench pixel devices were measured at the Institute of Microelectronics of the Chinese Academy of Sciences (IMECAS) at room temperature ( $20\ ^\circ\text{C}$ ) in a clean room. The setup for the measurement of IV and CV characteristics consists of a Keysight B1505A Power Device Analyzer coupled to a probe station and Keysight B2902A Source/Measure Unit. Tests have been performed on two devices, one is the device of Layout A21-21 ( $5\times 5$  pixel array with the pixel size of  $35\times 35\ \mu\text{m}$ ), the other one is the device of Layout A21-43 ( $3\times 3$  pixel array with the pixel size of  $25\times 25\ \mu\text{m}$ ).

Fig. 7a shows the measured reverse IV of these two devices and the simulated IV of a circular 3D-Trench device with a diameter of  $25\ \mu\text{m}$ , which has a comparable volume with the A21-43 device. The simulations agree well with the obtained results up to the onset of breakdown. The measured breakdown voltage is  $\sim 60\text{V}$ , whereas the simulations predict a lower breakdown voltage of  $\sim 46\text{V}$ , believed to be due to the difference in sharpness between the simulated and fabricated junction at the bottom of the cathode. The reverse leakage current of the 3D-Trench device of Layout A21-21 is less than  $1.22 \times 10^{-11}\text{A}$  and that of the device of Layout A21-43 is less than  $9.58 \times 10^{-12}\text{A}$  up to the bias voltage of  $20\text{V}$ .

Fig. 7b shows the measured CV of these two devices and the simulated CV of a circular 3D-Trench device with a diameter of  $25\ \mu\text{m}$ . The CV tests were performed using an AC signal amplitude of  $30\text{mV}$  and  $1\text{MHz}$  frequency. The measured result agrees well with the simulation. The measured saturated capacitance of these two devices are  $8.4 \times 10^{-14}\text{F}$  and  $4.2 \times 10^{-14}\text{F}$ , respectively. The extrapolated full depletion voltages are  $\sim 10\text{V}$ .

Fig. 8 shows the map of the leakage current of the A21-21 device on  $8''$  wafer before dicing. It can be seen that the largest leakage current is  $9.94 \times 10^{-9}\text{A}$ , and the smallest value is  $3.70 \times 10^{-11}\text{A}$ . The median is  $1.93 \times 10^{-10}\text{A}$  and the mean value is  $5.50 \times 10^{-10}\text{A}$ . The variance and standard deviation are  $2.80 \times 10^{-18}\text{A}$  and  $1.67 \times 10^{-9}\text{A}$ . The wafer-scale leakage current measured shows good uniformity and low dispersion, with a device yield of almost  $100\%$ .

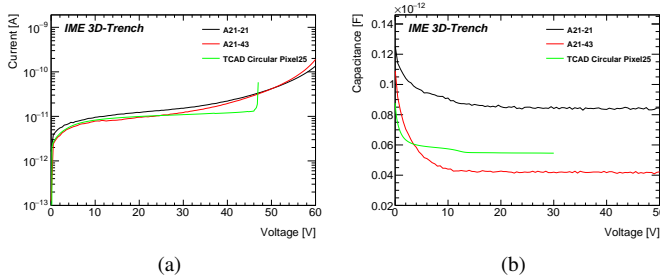


Fig. 7: (a) The measured reverse IV curves of 3D-Trench devices of the Layout A21-21 ( $5 \times 5$  pixel array with pixel size of  $35 \times 35\ \mu\text{m}$ ) and the Layout A21-43 ( $3 \times 3$  pixel array with pixel size of  $25 \times 25\ \mu\text{m}$ ) and the simulated IV curve of a circular 3D-Trench device with a diameter of  $25\ \mu\text{m}$ , (b) the measured and simulated reverse CV curves.

### B. Infrared Laser Illumination for CCE, Time Resolution and Rise Time

Measurements of the charge collection efficiency (CCE), time resolution and rise time of the 3D-Trench sensors were performed at the Rutherford Appleton Laboratory, using a customized Laser system operating in the infrared ( $\lambda = 1064\text{nm}$ ), capable to inject charge with a micron spatial resolution. The device under test (DUT) was mounted on a custom Transimpedance Amplifier COLA (Compact OPMD LGAD Amplifier, designed at the Oxford Physics Microstructure

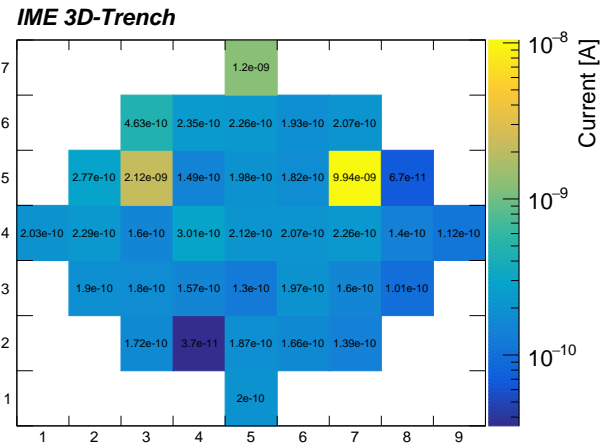


Fig. 8: Wafer uniformity.

Laboratory OPMD) board, which provides a gain of  $50\text{dB}$  up to  $1\text{GHz}$ , shown in Fig. 9. The sensor was biased by a Keithley 2410 HV Power Supply and signals were collected by a LeCroy WaveRunner 6100A Oscilloscope (Sampling Rate:  $5\text{GS/s}$ ,  $\sigma_{TDC} = 57.7\text{ps}$ ).

In this test, charge was injected using the IR laser at room temperature. Two devices were tested, one is the device of Layout A21-21, the other one is the device of Layout A21-43. Two different laser intensities were used for the test: Laser30 and Laser20, with the former of higher intensity and beam size big enough to illuminate the entire device array. Up to 15 pixels of the  $5 \times 5$  pixel array and 9 of the  $3 \times 3$  pixel array were connected to the TIA. Fig. 10 shows the normalized averaged signal waveforms at various bias voltages ranging from  $0$  to  $55\text{V}$ , all signal shapes agree well indicating its independence of the collected signal charge.



Fig. 9: The DUT is placed on a custom Transimpedance Amplifier (TIA) board designed at OPMD, the Compact OPMD LGAD Amplifier (COLA).

Fig. 11a shows the CCEs of these two 3D-Trench pixel sensors at the bias voltages ranging from  $0$  to  $50\text{V}$ . The

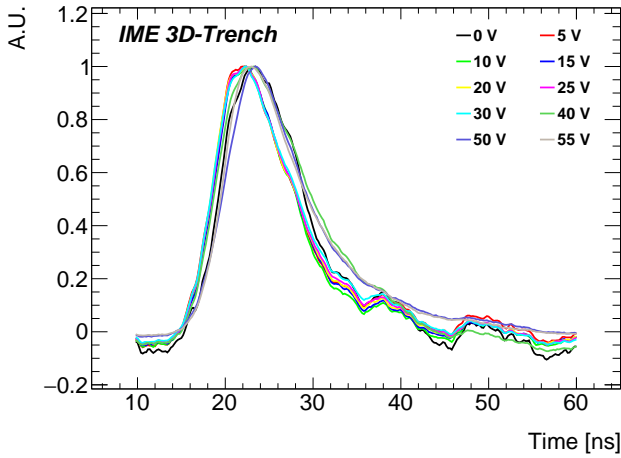


Fig. 10: The normalized averaged signal waveforms at various bias voltages ranging from 0 to 55 V.

collected charge is estimated by integration of the output pulse within a gating window and dividing the result by the nominal gain of the TIA. Since the full depletion is achieved at  $\sim 10$  V, the CCE does not increase significantly from 10 to 30 V. At the same laser intensity and bias voltage, the ratio between CCEs of the  $3 \times 3$  pixel sensor and the  $5 \times 5$  pixel sensor is  $\sim 30\%$  which is consistent with the ratio of their areas. Fig. 11b shows the CCEs of these two devices scaled to their own CCE at the bias voltage of 10 V. The steady increase from 10 V to 30 V is due to the drifting of holes in the weak electric field (the area far from the cathode), and the significant increase from 40 V to 50 V is due to the electron impact ionization in the cathode area where the electric field is high enough [31] to activate the electron impact ionization leading to charge multiplication. The pixel of the  $3 \times 3$  pixel sensor is smaller than the pixel of the  $5 \times 5$  pixel sensor, leading to an early onset of impact ionisation.

Preliminary tests were performed to measure the time resolution of the 3D-Trench sensor, from the standard deviation of the time interval between the laser trigger and a fixed threshold of the signal output. To compensate for the time walk effect, a Constant Fraction Discrimination (CFD) technique of threshold value of 30% was applied to the signal pulse. Fig. 12a shows the measured time resolutions of the  $3 \times 3$  pixel sensor and  $5 \times 5$  pixel sensor at the bias voltages ranging from 5 to 30 V at which the CCEs are relatively stable. Both devices show a time resolution of  $\sim 400$  ps or better, a value believed to be comparable to the inherent timing uncertainties of the laser system. More accurate timing measurements will be performed soon.

Fig. 12b shows the measured rise time defined as the time interval from 10% to 90% of the pulse height at the bias voltages ranging from 5 to 30 V. Both devices show a fast rise time ( $< 5.5$  ns) at the current charge injection scheme, and the measured rise time shows proportional relationship with the injected charge. Based on such fast rise time and the output of the amplifier returns to baseline within  $\sim 40$  ns, as shown in 10, this kind of 3D-Trench sensor has the capacity

to be used as a fast counting detector with the counting rate of  $\sim 2.5$  MHz or more.

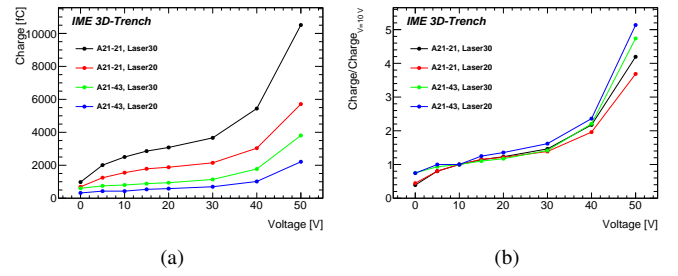


Fig. 11: (a) Collected charge at the bias voltage ranging from 0 to 50 V of the device of the Layout of A21-21 ( $5 \times 5$  pixel array with the pixel size of  $35 \times 35 \mu\text{m}$ ) and A21-43 ( $3 \times 3$  pixel array with the pixel size of  $25 \times 25 \mu\text{m}$ ), (b) Scale the collected charge to the charge collected at the bias voltage of 10 V.

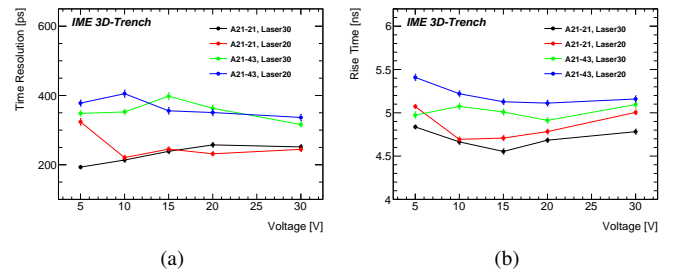


Fig. 12: (a) Time Resolution of the device of the Layout of A21-21 ( $5 \times 5$  pixel array with the pixel size of  $35 \times 35 \mu\text{m}$ ) and A21-43 ( $3 \times 3$  pixel array with the pixel size of  $25 \times 25 \mu\text{m}$ ), (b) Rise Time of these two devices.

## V. CONCLUSION AND FUTURE PLANS

A novel 3D-Trench sensor featuring a deep trench enclosing a central column electrode has been designed and successfully fabricated. The devices have been fabricated at the 8 inch COMS pilot line at the Institute of Microelectronics of the Chinese Academy of Sciences (IMECAS). The 3D-Trench devices were fabricated on a  $30 \mu\text{m}$  thick *p*-type epitaxial layer with a doping concentration of  $2 \times 10^{13} \text{ cm}^{-3}$  grown on the 8" wafer. Ultra-narrow etch width of  $0.5 \mu\text{m}$  and high aspect ratio  $> 70$  have been demonstrated. Initial IV, CV, CCE and timing measurements have been carried out at IMECAS and RAL. The preliminary results shown in this paper demonstrate that the devices are successfully working. Further tests are planned to investigate their characteristics in more detail and to further validate the matching between simulation and test results. Future devices, incorporating lessons learned from the current batch, are currently being designed.

## ACKNOWLEDGMENT

This work is supported by the National Key R&D Program of China under Grant 2023YFF0719600, General Program of

National Natural Science Foundation of China under Grant 12375188, and the Science and Technology Facilities Council (STFC) of United Kingdom under grants ST/S000747/1 and ST/W000547/1. We are also grateful for the support with equipment and technical personnel by the IMECAS, the School of Mathematical and Physical Sciences of the University of Sheffield, and the Rutherford Appleton Laboratory.

## REFERENCES

- [1] S. Parker, C. Kenney, and J. Segal, "3d — a proposed new architecture for solid-state radiation detectors," *Nuclear Instruments and Methods in Physics Research Section A: Accelerators, Spectrometers, Detectors and Associated Equipment*, vol. 395, no. 3, pp. 328–343, 1997, proceedings of the Third International Workshop on Semiconductor Pixel Detectors for Particles and X-rays. [Online]. Available: <https://www.sciencedirect.com/science/article/pii/S0168900297006943>
- [2] C. Kenney, S. Parker, J. Segal, and C. Stormont, "Silicon detectors with 3-d electrode arrays: fabrication and initial test results," *IEEE Transactions on Nuclear Science*, vol. 46, no. 4, pp. 1224–1236, 1999.
- [3] A. Heggelund, S. Huiberts, O. Dorholt, A. Read, O. Rohne, H. Sandaker, M. Lauritzen, B. Stugu, A. Kok, O. Koybasi, M. Povoli, M. Bomben, J. Lange, and A. Rummeler, "Radiation hard 3d silicon pixel sensors for use in the atlas detector at the hl-lhc," *Journal of Instrumentation*, vol. 17, no. 08, p. P08003, aug 2022. [Online]. Available: <https://dx.doi.org/10.1088/1748-0221/17/08/P08003>
- [4] D. V. Furelos, M. Carulla, E. Cavallaro, F. Förster, S. Grinstein, J. Lange, I. L. Paz, M. Manna, G. Pellegrini, D. Quirion, and S. Terzo, "3d sensors for the hl-lhc," *Journal of Instrumentation*, vol. 12, no. 01, p. C01026, jan 2017. [Online]. Available: <https://dx.doi.org/10.1088/1748-0221/12/01/C01026>
- [5] J. Lange, M. C. Areste, E. Cavallaro, F. Förster, S. Grinstein, I. L. Paz, M. Manna, G. Pellegrini, D. Quirion, S. Terzo, and D. V. Furelos, "3d silicon pixel detectors for the high-luminosity lhc," *Journal of Instrumentation*, vol. 11, no. 11, p. C11024, nov 2016. [Online]. Available: <https://dx.doi.org/10.1088/1748-0221/11/11/C11024>
- [6] C. Guardiola, D. Quirion, G. Pellegrini, C. Fleta, S. Esteban, M. A. Cortés-Giraldo, F. Gómez, T. Solberg, A. Carabe, and M. Lozano, "Silicon-based three-dimensional microstructures for radiation dosimetry in hadrontherapy," *Applied Physics Letters*, vol. 107, no. 2, p. 023505, 07 2015. [Online]. Available: <https://doi.org/10.1063/1.4926962>
- [7] D. Bachiller-Perea, J. G. López, M. d. C. Jiménez-Ramos, F. Gómez, C. Fleta, D. Quirion, A. García-Osuna, and C. Guardiola, "Characterization of the charge collection efficiency in silicon 3-d-detectors for microdosimetry," *IEEE Transactions on Instrumentation and Measurement*, vol. 70, pp. 1–11, 2021.
- [8] D. Bachiller-Perea, M. Zhang, C. Fleta, D. Quirion, D. Bassignana, F. Gómez, and C. Guardiola, "Microdosimetry performance of the first multi-arrays of 3d-cylindrical microdetectors," *Scientific Reports*, vol. 12, no. 1, p. 12240, 2022. [Online]. Available: <https://doi.org/10.1038/s41598-022-14940-1>
- [9] T. Ariyoshi and T. Matsunaga, "Balanced high detection efficiency and rapid detection response in a silicon trench hard x-ray photon sensor," *IEEE Sensors Journal*, vol. 23, no. 20, pp. 24 465–24 472, 2023.
- [10] L. T. Tran, L. Chartier, D. A. Prokopovich, D. Bolst, M. Povoli, A. Summanwar, A. Kok, A. Pogossow, M. Petasecca, S. Guatelli, M. I. Reinhard, M. Lerch, M. Nancarrov, N. Matsufuji, M. Jackson, and A. B. Rosenfeld, "Thin silicon microdosimeter utilizing 3-d mems fabrication technology: Charge collection study and its application in mixed radiation fields," *IEEE Transactions on Nuclear Science*, vol. 65, no. 1, pp. 467–472, 2018.
- [11] G. Paternoster, G. Borghi, M. Boscardin, N. Cartiglia, M. Ferrero, F. Ficorella, F. Siviero, A. Gola, and P. Bellutti, "Trench-isolated low gain avalanche diodes (ti-lgads)," *IEEE Electron Device Letters*, vol. 41, no. 6, pp. 884–887, 2020.
- [12] S. Shimada, Y. Otake, S. Yoshida, Y. Jibiki, M. Fujii, S. Endo, R. Nakamura, H. Tsugawa, Y. Fujisaki, K. Yokochi, J. Iwase, K. Takabayashi, H. Maeda, K. Sugihara, K. Yamamoto, M. Ono, K. Ishibashi, S. Matsumoto, H. Hiyama, and T. Wakano, "A spad depth sensor robust against ambient light: The importance of pixel scaling and demonstration of a 2.5 $\mu\text{m}$  pixel with 21.8% pde at 940nm," in *2022 International Electron Devices Meeting (IEDM)*, 2022, pp. 37.3.1–37.3.4.
- [13] G. Pellegrini, M. Manna, and D. Quirion, "3d-si single sided sensors for the innermost layer of the atlas pixel upgrade," *Nuclear Instruments and Methods in Physics Research Section A: Accelerators, Spectrometers, Detectors and Associated Equipment*, vol. 924, pp. 69–72, 2019, 11th International Hiroshima Symposium on Development and Application of Semiconductor Tracking Detectors. [Online]. Available: <https://www.sciencedirect.com/science/article/pii/S016890021830723X>
- [14] S. Terzo, J. Carlotto, S. Grinstein, M. Manna, G. Pellegrini, and D. Quirion, "Performance of radiation hard 3d pixel sensors for the upgrade of the atlas inner tracker," *Journal of Physics: Conference Series*, vol. 2374, no. 1, p. 012168, nov 2022. [Online]. Available: <https://dx.doi.org/10.1088/1742-6596/2374/1/012168>
- [15] L. Diehl, S. Argyropoulos, O. Ferrer, M. Hauser, K. Jakobs, M. King, F. Lex, G. Kramberger, U. Parzefall, G. Pellegrini, C. Schwemmbauer, and D. Sperllich, "Evaluation of 3d sensors for fast timing applications," *Nuclear Instruments and Methods in Physics Research Section A: Accelerators, Spectrometers, Detectors and Associated Equipment*, vol. 1065, p. 169517, 2024. [Online]. Available: <https://www.sciencedirect.com/science/article/pii/S0168900224004431>
- [16] O. Dorholt, T. Hansen, A. Heggelund, A. Kok, N. Pacifico, O. Rohne, H. Sandaker, B. Stugu, Z. Yang, M. Bomben, A. Rummeler, and J. Weingarten, "Beam tests of silicon pixel 3d-sensors developed at sintef," *Journal of Instrumentation*, vol. 13, no. 08, p. P08020, aug 2018. [Online]. Available: <https://dx.doi.org/10.1088/1748-0221/13/08/P08020>
- [17] S. Terzo, M. Boscardin, J. Carlotto, G.-F. Dalla Betta, G. Darbo, O. Dorholt, F. Ficorella, G. Gariano, C. Gemme, G. Giannini, S. Grinstein, A. Heggelund, S. Huiberts, A. Kok, O. Koybasi, A. Lapertosa, M. E. Lauritzen, M. Manna, R. Mendicino, H. Oide, G. Pellegrini, M. Povoli, D. Quirion, O. M. Rohne, S. Ronchin, H. Sandaker, M. A. Abdulla Samy, B. Stugu, and L. Vannoli, "Novel 3d pixel sensors for the upgrade of the atlas inner tracker," *Front. Phys.*, vol. 9, p. 624668, 2021.
- [18] A. Kok, M. Boscardin, G.-F. D. Betta, C. Da Via, G. Darbo, C. Fleta, T.-E. Hansen, J. Hasi, C. Kenney, N. Lietaer, M. Lozano, S. I. Parker, G. Pellegrini, and A. Summanwar, "Results from the first prototype of large 3d active edge sensors," in *2011 IEEE Nuclear Science Symposium Conference Record*, 2011, pp. 1319–1323.
- [19] G.-F. Dalla Betta and J. Ye, "Silicon radiation detector technologies: From planar to 3d," *Chips*, vol. 2, no. 2, pp. 83–101, 2023. [Online]. Available: <https://www.mdpi.com/2674-0729/2/2/6>
- [20] P. Grenier, G. Alimonti, M. Barbero, R. Bates, E. Bolle, M. Borri, M. Boscardin, C. Buttar, M. Capua, M. Cavalli-Sforza, M. Cobal, A. Cristofoli, G.-F. Dalla Betta, G. Darbo, C. Da Via, E. Devetak, B. DeWilde, B. Di Girolamo, D. Dobos, K. Einsweiler, D. Esseni, S. Fazio, C. Fleta, J. Freestone, C. Gallrapp, M. Garcia-Sciveres, G. Gariano, C. Gemme, M.-P. Giordani, H. Gjersdal, S. Grinstein, T. Hansen, T.-E. Hansen, P. Hansson, J. Hasi, K. Helle, M. Hoferkamp, F. Hüggling, P. Jackson, K. Jakobs, J. Kalliopuska, M. Karagounis, C. Kenney, M. Köhler, M. Kocian, A. Kok, S. Kolya, I. Korokolov, V. Kostyukhin, H. Krüger, A. La Rosa, C. Lai, N. Lietaer, M. Lozano, A. Mastroberardino, A. Micelli, C. Nellist, A. Oja, V. Oshea, C. Padilla, P. Palestri, S. Parker, U. Parzefall, J. Pater, G. Pellegrini, H. Pernegger, C. Piemonte, S. Pospisil, M. Povoli, S. Roe, O. Rohne, S. Ronchin, A. Rovani, E. Ruscinio, H. Sandaker, S. Seidel, L. Selmi, D. Silverstein, K. Sjøbæk, T. Slavicek, S. Stapnes, B. Stugu, J. Stupak, D. Su, G. Susinno, R. Thompson, J.-W. Tsung, D. Tsybychev, S. Watts, N. Wermes, C. Young, and N. Zorzi, "Test beam results of 3d silicon pixel sensors for the atlas upgrade," *Nuclear Instruments and Methods in Physics Research Section A: Accelerators, Spectrometers, Detectors and Associated Equipment*, vol. 638, no. 1, pp. 33–40, 2011. [Online]. Available: <https://www.sciencedirect.com/science/article/pii/S0168900211003524>
- [21] G. Giacomini, A. Bagolini, M. Boscardin, G.-F. Dalla Betta, F. Mattedi, M. Povoli, E. Vianello, and N. Zorzi, "Development of double-sided full-passing-column 3d sensors at fbk," *IEEE Transactions on Nuclear Science*, vol. 60, no. 3, pp. 2357–2366, 2013.
- [22] A. Zoboli, M. Boscardin, L. Bosisio, G.-F. Dalla Betta, C. Piemonte, S. Ronchin, and N. Zorzi, "Double-sided, double-type-column 3-d detectors: Design, fabrication, and technology evaluation," *IEEE Transactions on Nuclear Science*, vol. 55, no. 5, pp. 2775–2784, 2008.
- [23] G.-F. D. Betta, A. Bagolini, M. Boscardin, L. Bosisio, P. Gabos, G. Giacomini, C. Piemonte, M. Povoli, E. Vianello, and N. Zorzi, "Development of modified 3d detectors at fbk," in *IEEE Nuclear Science Symposium & Medical Imaging Conference*, 2010, pp. 382–387.
- [24] D. Sultan, G.-F. D. Betta, R. Mendicino, M. Boscardin, S. Ronchin, and N. Zorzi, "First production of new thin 3d sensors for hl-lhc at fbk," *Journal of Instrumentation*, vol. 12, no. 01, p. C01022, jan

2017. [Online]. Available: <https://dx.doi.org/10.1088/1748-0221/12/01/C01022>
- [25] Z. Li, “New bnl 3d-trench electrode si detectors for radiation hard detectors for slhc and for x-ray applications,” *Nuclear Instruments and Methods in Physics Research Section A: Accelerators, Spectrometers, Detectors and Associated Equipment*, vol. 658, no. 1, pp. 90–97, 2011, rESMDD 2010. [Online]. Available: <https://www.sciencedirect.com/science/article/pii/S0168900211008473>
- [26] L. Diehl, O. Ferrer, M. Hauser, K. Jakobs, M. King, G. Kramberger, N. Moffat, U. Parzefall, G. Pellegrini, and D. Sperlich, “Investigation of the time resolution of 3d silicon sensors,” *Journal of Instrumentation*, vol. 17, no. 12, p. C12003, dec 2022. [Online]. Available: <https://dx.doi.org/10.1088/1748-0221/17/12/C12003>
- [27] S. Terzo, S. Grinstein, M. Manna, G. Pellegrini, and D. Quirion, “A new generation of radiation hard 3d pixel sensors for the atlas upgrade,” *Nuclear Instruments and Methods in Physics Research Section A: Accelerators, Spectrometers, Detectors and Associated Equipment*, vol. 982, p. 164587, 2020. [Online]. Available: <https://www.sciencedirect.com/science/article/pii/S0168900220309840>
- [28] G.-F. Dalla Betta, M. Boscardin, M. Bomben, M. Brianzi, G. Calderini, G. Darbo, R. Dell’Orso, A. Gaudiello, G. Giacomini, R. Mendicino, M. Meschini, A. Messineo, S. Ronchin, D. Sultan, and N. Zorzi, “The infn-fbk “phase-2” r&d program,” *Nuclear Instruments and Methods in Physics Research Section A: Accelerators, Spectrometers, Detectors and Associated Equipment*, vol. 824, pp. 388–391, 2016, frontier Detectors for Frontier Physics: Proceedings of the 13th Pisa Meeting on Advanced Detectors. [Online]. Available: <https://www.sciencedirect.com/science/article/pii/S0168900215010463>
- [29] M. Liu, S. Lu, and Z. Li, “Theoretical bases of hypothetical sphere-electrode detectors and practical near-sphere-electrode (semisphere-electrode and near-semisphere-electrode) detectors,” *Journal of Physics D: Applied Physics*, vol. 54, no. 4, p. 045101, nov 2020. [Online]. Available: <https://dx.doi.org/10.1088/1361-6463/abbe48>
- [30] “Synopsis,” <https://www.synopsys.com/manufacturing/tcad.html>.
- [31] M. Ershov and V. Ryzhii, “Temperature dependence of the electron impact ionization coefficient in silicon,” *Semiconductor Science and Technology*, vol. 10, no. 2, p. 138, feb 1995. [Online]. Available: <https://dx.doi.org/10.1088/0268-1242/10/2/003>

**Manwen Liu** is currently a junior faculty at the Key Laboratory of Fabrication Technologies for Integrated Circuits of the Chinese Academy of Sciences and the Institute of Microelectronics of the Chinese Academy of Sciences (IMECAS). She received her B.S. and Ph.D. degrees in Xiangtan University, Xiangtan, China, in 2014 and 2019, respectively. Her main research interests are radiation and optical detectors.

**Zhihua Li** is currently a senior faculty at the Key Laboratory of Fabrication Technologies for Integrated Circuits of the Chinese Academy of Sciences and the Institute of Microelectronics of the Chinese Academy of Sciences (IMECAS) in Beijing, China.

**Jun Luo** is currently a senior faculty at the Key Laboratory of Fabrication Technologies for Integrated Circuits of the Chinese Academy of Sciences and the Institute of Microelectronics of the Chinese Academy of Sciences (IMECAS) in Beijing, China.

**Huimin Ji** is currently a PhD student at the Key Laboratory of Fabrication Technologies for Integrated Circuits of the Chinese Academy of Sciences, Institute of Microelectronics of the Chinese Academy of Sciences (IMECAS) and the University of Chinese Academy of Sciences, Beijing, China. She received her B.S. degree in Beijing Information Science and Technology University, Beijing, China.

**Le Zhang** is currently a graduate student at the Key Laboratory of Fabrication Technologies for Integrated Circuits of the Chinese Academy of Sciences, Institute of Microelectronics of the Chinese Academy of Sciences (IMECAS) and the University of Chinese Academy of Sciences in Beijing, China.

**Wenzheng Cheng** is currently a graduate student at the Key Laboratory of Fabrication Technologies for Integrated Circuits of the Chinese Academy of Sciences, Institute of Microelectronics of the Chinese Academy of Sciences (IMECAS) and the University of Chinese Academy of Sciences in Beijing, China. He received his B.S. degree in Xiangtan University, Xiangtan, China.

**Zheng Li** is currently a professor at Ludong University in Yantai and a visiting researcher at Institute of Microelectronics of the Chinese Academy of Sciences (IMECAS), Beijing, China.

**Bo Tang** is currently a senior faculty at the Key Laboratory of Fabrication Technologies for Integrated Circuits of the Chinese Academy of Sciences and the Institute of Microelectronics of the Chinese Academy of Sciences (IMECAS) in Beijing, China.

**Peng Zhang** is currently a junior faculty at the Key Laboratory of Fabrication Technologies for Integrated Circuits of the Chinese Academy of Sciences and the Institute of Microelectronics of the Chinese Academy of Sciences (IMECAS) in Beijing, China.

**Jing Wen** is currently a junior faculty at the Key Laboratory of Fabrication Technologies for Integrated Circuits of the Chinese Academy of Sciences and the Institute of Microelectronics of the Chinese Academy of Sciences (IMECAS) in Beijing, China.

**Jiaxiang Sun** is currently a graduate student at Ludong University in Yantai, China.

**Trevor Vickey** received a PhD in physics from the University of Illinois, Urbana-Champaign, USA in 2004. He is currently a senior faculty member at the University of Sheffield, Sheffield, UK.

**E. Giulio Villani** received the Degree in electronic engineering from the University of Bologna, Bologna, Italy, in 1995. He joined the Particle Physics Department, Rutherford Appleton Laboratory of the Science and Technology Facilities Council (STFC), Oxfordshire, U.K., in 2001. He is involved in modeling and simulations of semiconductor devices for particle physics applications.

**Dengfeng Zhang** received the B.S. degree in applied physics and B.E. in software engineering from Shandong University, Weihai, Shandong, China, in 2013 and the Ph.D. degree in particle physics and nuclear physics from Shandong University, Jinan, Shandong, China, in 2018.

He is currently a postdoctoral research fellow at the University of Sheffield, Sheffield, UK.